Plasma Science and Technology

PAPER

Plasma density measurement and downstream etching of silicon and silicon oxide in Ar/NF_3 mixture remote plasma source

Plasma Sci. Technol. **21** (2019) 064007 (6pp) https://doi.org/10.1088/2058-6272/ab0bd3

Plasma density measurement and downstream etching of silicon and silicon oxide in Ar/NF_3 mixture remote plasma source

H J YEOM[1], D H CHOI[1], Y S LEE[2], J H KIM[1], D J SEONG[1], S J YOU[2,3] and H C LEE[1,3]

[1] Korea Research Institute of Standards and Science (KRISS), Daejeon 34113, Republic of Korea
[2] Department of Physics, Chungnam National University, Daejeon 34134, Republic of Korea

E-mail: sjyou@cnu.ac.kr and LHC@kriss.re.kr

Received 30 September 2018, revised 28 February 2019
Accepted for publication 1 March 2019
Published 26 April 2019

Abstract

In this study, plasma density measurements were performed near the plume region of the remote plasma source (RPS) in Ar/NF_3 gas mixtures using a microwave cutoff probe. The measured plasma density is in the range of 10^{10}–10^{11} cm^{-3} in the discharge conditions with RPS powers of 2–4 kW and gas pressures of 0.87–4 Torr. The plasma density decreased with increasing gas pressures and RPS powers under various Ar/NF_3 mixing ratios. This decrease in the plasma density measured at the fixed measurement position (plume region) can be understood by the reduction of the electron energy relaxation length with increases in the gas pressures and mixing ratio of $NF_3/(Ar/NF_3)$. We also performed downstream etching of silicon and silicon oxide films in this system. The etch rate of the silicon films significantly increases while the silicon oxide is slightly etched with the gas pressures and powers. It was also found that the etch rate strongly depends on the wafer position on the processing chamber electrode, and that the etch selectivity reached 96–131 in the discharge conditions of RF powers (3730–4180 W) and gas pressures (3.6–4 Torr).

Keywords: remote plasma source, electron density, cutoff probe, downstream etch

(Some figures may appear in colour only in the online journal)

1. Introduction

Remote plasma sources (RPSs) have often been used in industrial semiconductor and display processing, such as etching and deposition. As the line width of the critical dimension in recent plasma processing with three-dimensional device structures shrinks, RPSs are of remarkable interest because the RPS, which generates and transports the reactive radicals with blocking the charged species (electrons and ions) into the downstream processing chamber, allows a damage-free etching process, such as cleaning residues remaining in the chamber after processing of materials such as silicon, silicon oxide, tungsten [1–3]. RPSs can be made from many different plasma generation types, such as inductive discharge, capacitive discharge, and ferromagnetic inductively coupled plasma (ICP), etc. Among such types, the ferromagnetic ICP type has been widely used as a RPS in recent industry because of its high plasma density and temperature archiving high gas dissociation rate [4–6].

In etching processes including conventional and remote plasma etching, fluorine atoms are typical main etchants for silicon-based materials such as Si, SiO_2, SiN, and Si_3N_4, etc. Many fluorocarbon gases, such as CF_4 and C_2F_6, C_4F_8 have been used in etching and cleaning processes. However, these gases can create a fluorocarbon polymer layer that may contaminate the chamber or wafer surface. There is an alternative

[3] Authors to whom any correspondence should be addressed.

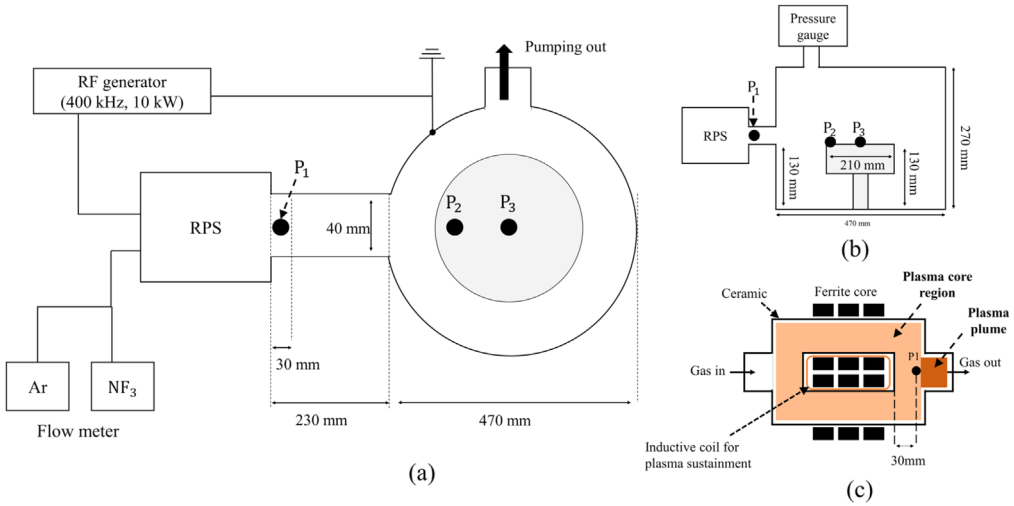

Figure 1. Schematic of the experimental setup: (a) view from above, (b) cross section view, (c) RPS.

gas to overcome this concern: nitrogen trifluoride, NF_3, which hardly forms a polymer layer and creates many F atoms due to its very high dissociation rate in plasmas. NF_3 also has environmental benefits because it has a shorter atmospheric lifetime than fluorocarbon [3].

In NF_3 RPS plasmas, electron density is a key parameter in downstream etching and cleaning, even though the electrons cannot reach the main processing chamber. This is because the higher plasma density in the RPS plasma allows it to create more radical species and to heat up the radical's temperature, which directly affects the processing results. Therefore, measurement of the electron density is highly important in terms of the fundamental understanding of both the RPS plasma and industrial applications. In addition, the database of the plasma density in the RPS plasmas can be used as a simulation benchmark, elaborating the accuracy of simulation.

Typical methods for measuring electron density are Langmuir probes, optical emission spectrometry (OES), and microwave cutoff probes. A Langmuir probe has some limitations in terms of being applied in RPS plasma processing due to the etching and deposition of the probe tip and RF noise in circumstances in which the RPS uses high discharge powers. The OES method also has a limitation that it is difficult to measure the absolute electron density in complex gas mixtures. Among the methods, the microwave cutoff probe is one of the novel ones, with less complex equations and assumptions as well as a high measurement accuracy for electron density measurement; it is also possible to measure the electron density even when a nonconductive film is deposited by the processing gases [7]. However, there have been few studies on the measurement of electron density in RPS plasmas. This is due to a number of reasons, such as the high temperature of radicals and the extremely high radical density causing probe damage (melting and etching) and geometric limitation for measurement.

In this study, we measured electron density in the plume region of RPS plasmas in a Ar/NF_3 mixture gas by using a cutoff probe. Because the high density and temperature plasmas are generated inside the RPS, a ceramic shield cutoff probe [8] was applied in this study. Also, we measured the etch rates and selectivity of Si and SiO_2 films in the RPS system.

2. Experimental setup

2.1. Schematic diagram of the chamber

Figures 1(a) and (b) present an experimental setup of the downstream chamber system with the RPS. The fluorine radicals generated by the RPS plasma are transported through a pipe of 230 mm in length and reach to the downstream chamber. The downstream chamber has a cylindrical shape with a height of 270 mm and inner diameter of 470 mm. Gas pressure was measured in the downstream chamber through a capacitive diaphragm gauge. The plasma was generated by a ferromagnetic ICP type RPS [5]. A schematic of the RPS is shown in figure 1(c). The RPS has a cylindrical ceramic chamber enclosed by a ferrite core, and a coil wound around the inner ferrite core. In this experiment, a ferromagnetic ICP was used for the RPS. For a ferromagnetic ICP, power is applied to the coil to generate plasma in the same way as a conventional ICP. However, the ferromagnetic ICP has high power transfer efficiency between the coil and plasma due to the ferrite material having high permeability. This results in a higher plasma density than conventional ICPs. The plasma is generated around the coil located inside the RPS. Under high pressure conditions, the plasma exists only near the RPS due to local electron kinetics. In figure 1(c), the plasma core area and plasma plume are shown in an orange color. A RF power of driving frequency 400 kHz is applied to the inductive coil, and the Ar/NF_3 mixture gas is injected into the RPS through each mass flow meter. This RPS is a commercial equipment that uses a load-dependent power supplying method that relies on load impedance, where the power increases as the gas flow rate increases. Therefore, if we want to increase the RF power, the gas pressure should be increased at the same time.

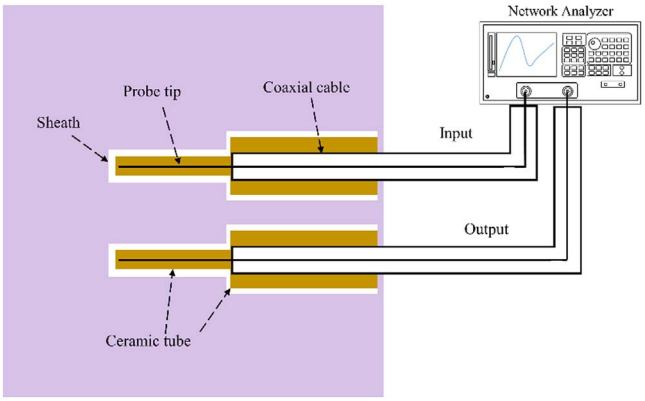

Figure 2. Schematic drawing of a ceramic shielded cutoff probe system.

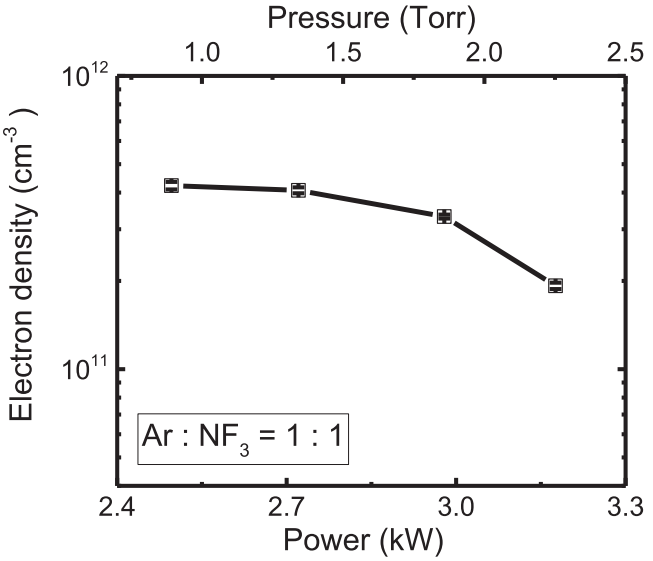

Figure 3. The measured plasma density as a function of power and pressure at a Ar:NF_3 = 1:1 mixing ratio.

The pressures used in the experiment were in the range of 0.87–4 Torr and the powers were in the range of 2.1–4.2 kW. The plasma density was measured at position 1 (P_1), the RPS plume region, and the Si and SiO_2 samples were placed at position 2 (P_2) and position 3 (P_3) as shown in figures 1(a) and (b). The RPS equipment is connected at the side of the processing chamber so that P_2 at the substrate edge is close to the RPS. Therefore, the density of F radicals reaching at P_2 is higher than that at P_3.

2.2. Cutoff probe for plasma density measurement

In this experiment, plasma density is measured using a microwave cutoff probe. The wave-cutoff method for measurement of the absolute electron density was developed by Kim *et al* [7]. Using a radiating and detecting antenna with a network analyzer, the transmission spectrum is measured and analyzed to determine the cutoff frequency. The electron density has the following relationship with the cutoff frequency [9]

$$\omega_{\mathrm{p}}^2 = \frac{e^2 n_{\mathrm{e}}}{\epsilon_0 m_{\mathrm{e}}} \tag{1}$$

where n_{e} is the electron density and m_{e} is the mass of electrons. Due to its simple equation without any specific assumptions, the cutoff method provides high accuracy in the measurement of absolute electron density. However, when measuring plasma density in the RPS, it is difficult to measure with conventional cutoff probes because of the probe tip etching or melting due to the high temperature and the density of the radicals. Thus, a method of measuring the cutoff probe in circumstances of high temperature and density needs to be adapted. Thus, we used a recently developed method, wrapping the conventional cutoff probe with a ceramic tube [8], in this RPS plasma diagnostic study, as shown in figure 2. This confirmed that there were few measurement errors with a ceramic shield.

3. Results and discussion

3.1. Plasma density measurement

The experiment was performed in the plume region of the RPS under various powers, pressures and gas mixing ratios. Figure 3 shows the measured electron density with RF powers and gas pressures at P_1 of the plume region for the gas mixing ratio of Ar:NF_3 = 1:1. The measured plasma density was $4.23 \times 10^{11}\,\mathrm{cm}^{-3}$ at a pressure of 0.87 Torr and a power of 2.49 kW. As the pressure and power were increased, the measured plasma density gradually decreased, and thus, the plasma density reached $1.92 \times 10^{11}\,\mathrm{cm}^{-3}$ at the discharge conditions of 2.3 Torr in pressure and 3.17 kW power. According to the power balance equation in the zero-dimensional fluid model [10], the plasma density should increase when the RF power is increased. In the measurement results, however, the plasma density decreases with respect to the powers and pressures. The reason for this decrease is that the measurement position is fixed in the plume region. In fact, the electron density in the RPS core region can be increased with the RF powers and gas pressures. However, as the gas pressure increases, there are a number of collisions between electrons and neutrons, such as momentum transfer, excitations, and ionizations. Thus, the electron density measured at P_1 of the plume region is expected to decrease.

The decrease in the plasma density at the fixed measurement position can be understood by the local electron kinetics effect. At low gas pressure where the electron energy relaxation length λ_ϵ is longer than the chamber length L, the electrons generated and heated in the RPS core region where electron heating occurs can reach the plume region. This is called nonlocal electron kinetics, where the ionization process occurs in the entire discharge region [11–13]. However, as the gas pressure increases, the heated electrons lose their energy through electron-neutral collisions. Thus, λ_ϵ becomes shorter than the L. This is termed local electron kinetics, where the

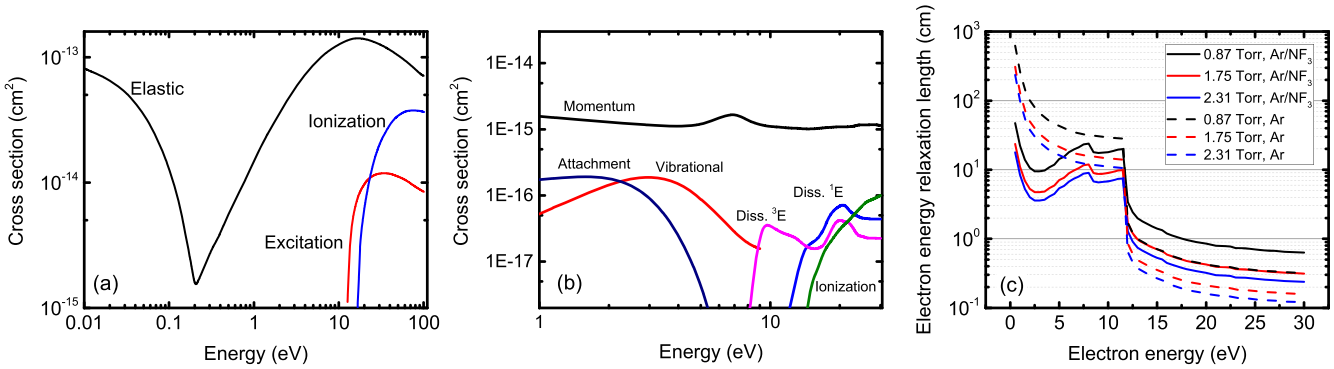

Figure 4. Electron-neutral collision cross sections of (a) Ar, (b) NF_3 and (c) calculation of λ_ϵ for pure Ar and Ar/NF_3 mixture gases.

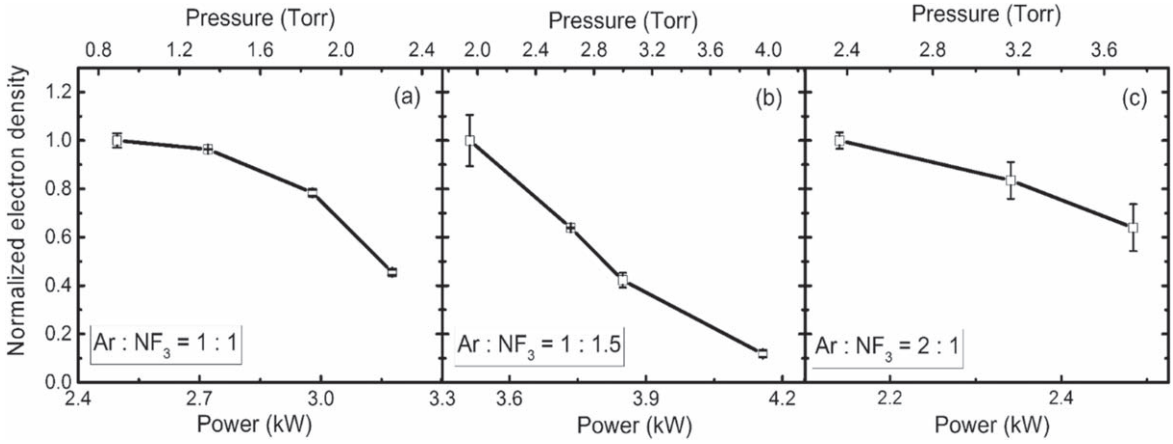

Figure 5. Normalized electron density with RF powers and gas pressures under various gas mixing ratios. (a) Ar:NF_3 = 1:1, (b) Ar:NF_3 = 1:1.5 and (c) Ar:NF_3 = 2:1.

electron heating region is identical to the ionization region [11–13]. The transition from nonlocal to local kinetics occurs when the external parameters are changed, such as the gas pressure [11–13], antenna size [14, 15], or the addition of molecule gas [16]. In this RPS experiment, the electron kinetic regime can be confirmed by comparing the λ_ϵ with the chamber dimension. Figure 4(c) shows the calculated λ_ϵ. Here, the λ_ϵ is given, as in reference [10]

$$\lambda_\epsilon = \frac{v}{\sqrt{3\nu_m \nu_{ine}}} \tag{2}$$

where ν_m and ν_{ine} are the electron collision frequencies for momentum transfer collisions and inelastic collisions, which were obtained from the collision cross sections of the Ar and NF_3 [17–23] in figures 4(a) and (b). The λ_ϵ depends on momentum transfer collisions and inelastic collisions. As shown in figure 4(a), the excitation and ionization collisions of the Ar occur in the relatively high electron energy region above the threshold energy of 11.56 eV. In the case of NF_3, however, there are a lot of collisions in the low electron energy region below 11.56 eV due to attachment, vibrational, and dissociative excitations. Therefore, the λ_ϵ even in low electron energy will be very short when NF_3 is mixed. This can be proved by figure 4(c). The λ_ϵ in the entire electron energy region decreases with the increasing gas pressure. For example, the λ_ϵ changed from 1.33 cm to 0.5 cm at the

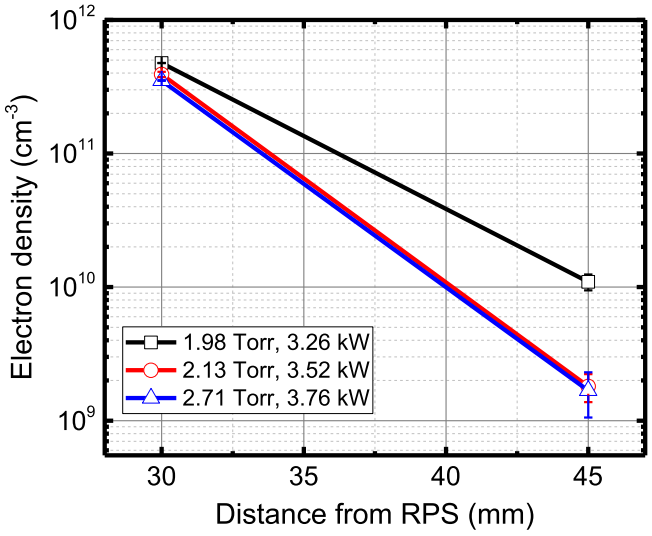

Figure 6. Electron density as a function of measurement position from the RPS at various pressures and power conditions.

electron energy of 15.7 eV, which is responsible for the ionization of the Ar. This λ_ϵ is much shorter than the distance from the core to the plume. Besides, it can be seen that the λ_ϵ of the low energy region is strongly reduced with the gas pressures at the discharge of the Ar/NF_3 mixture gas,

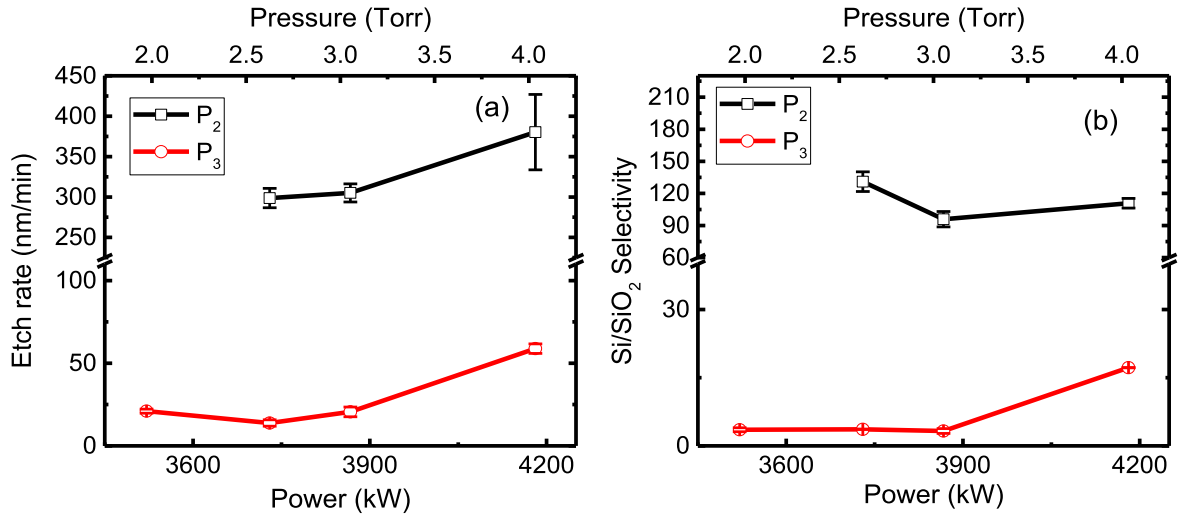

Figure 7. (a) Si etch rate and (b) selectivity of Si to SiO_2 at the P_2 and P_3 positions.

compared to the pure Ar gas in figure 4(c). The λ_ϵ at the electron energy of 3 eV decreased from 9.5 cm to 3.5 cm. That is, the energetic electrons heated in the RPS core do not reach the measurement position in this experiment, and the cooled electrons via collision processes are just diffused into the plume region.

Figure 5 shows the normalized electron density results measured at P_1 under various gas mixing ratios: (a) $Ar:NF_3 = 1:1$, (b) $Ar:NF_3 = 1:1.5$ and (c) $Ar:NF_3 = 2:1$. The plasma density in the gas mixture of $Ar:NF_3 = 1:1.5$ decreases more rapidly than in the case of $Ar:NF_3 = 1:1$, as the gas pressure increases. On the other hand, the plasma density with a higher portion of the Ar flow rate ($Ar:NF_3 = 2:1$) results in less density decrease than in the case of $Ar:NF_3 = 1:1$. This result is mainly due to the remarkable reduction of the λ_ϵ with the enhanced mixing ratio of the NF_3. Also, the pressure gradient between the RPS core and the plume region can occur at high flow rates [24], and thus, a greater decrease in the λ_ϵ is expected in this experimental condition.

Figure 6 shows the electron density as a function of the measurement position. Here, the 30 mm indicates P_1, and the 45 mm indicates the position with a 15 mm distance from P_1 at the $Ar:NF_3 = 1:1$ condition. The electron density measured at P_1 was 4.65×10^{11} cm^{-3} at 1.98 Torr, 3.89×10^{11} cm^{-3} at 2.13 Torr and 3.5×10^{11} cm^{-3} at 2.71 Torr. As the pressures increases, the density difference between the two positions (30 mm, 45 mm) increases significantly mainly due to the reduction of the $\boldsymbol{\lambda_\epsilon}$, as discussed before.

3.2. Downstream etching of silicon and silicon oxide

In this work, the etch rates of Si and SiO_2 and their selectivity were measured as a function of the RF powers and gas pressures. We used Si coupon wafers with a single crystal Si $\langle 111 \rangle$ for the Si etching experiment, while armophose SiO_2 film with a 100 nm thickness was deposited on the Si wafer using commercial low-pressure chemical vapor deposition equipment. These sample wafers are placed onto P_2 and P_3 of the lower electrode in the main processing chamber, as indicated in figure 1.

Figures 7(a) and (b) show the Si etch rate and Si/SiO_2 selectivity depending on the distance to the RPS at the fixed mixing ratio of $Ar:NF_3 = 1:1.5$. It was found that the Si wafers are significantly etched with the RF powers and gas pressures, while the SiO_2 films are slightly etched. At P_2, the etch rate of the Si wafer was about 298–380 nm min^{-1} with the RF powers and gas pressures, and the selectivity was 95–131. At P_3, the etch rate of the Si wafer was 13.8–58.8 nm min^{-1} and selectivity was 3–17. Thus, the etch rate of the Si wafer at P_2 is 5–10 times higher than that at P_3. This can be understood by the reduction of the F radical density and decrease in the gas temperature as the wafers move away from the RPS [6, 25–29].

4. Conclusion

In this study, we measured the electron density in Ar/NF_3 mixture RPS plasmas at various pressures, powers, gas flow rates, and distances. To measure the electron density, a ceramic shielded microwave cutoff probe was used. The measured plasma density is in the range of 10^{10}–10^{11} cm^{-3} in the plume region of the PRS with RF powers of 2–4 kW and gas pressures of 0.87–4 Torr. It was found that the plasma density decreased with the increasing gas pressures and RPS powers under various Ar/NF_3 mixing ratios due to the reduction of the electron energy relaxation length. We also investigated the Si, SiO_2 etch rates and their selectivity in the downstream chamber depending on the sample location. The Si wafers were significantly etched with the RF powers and gas pressures, while the SiO_2 films were slightly etched. The etch selectivity was significantly influenced by the wafer sample locations. These results for the electron density and the etch rate in the RPS system are expected to be helpful both for industrial etching processes using RPSs and for simulation benchmarking.

Acknowledgments

This research was supported by the Korea Research Institute of Standard and Science (KRISS) and the R&D Convergence Program (1711062007, CAP-17–02-NFRI-01) of the National Research Council of Science and Technology (NST) of Republic of Korea.

ORCID iDs

H C LEE https://orcid.org/0000-0003-2754-1512

References

[1] Blain M G, Jarecki R L and Simonson R J 1998 *J. Vac. Sci. Technol.* A **16** 2115
[2] Nagata A *et al* 1989 *Jpn. J. Appl. Phys.* **28** 2368
[3] Kastenmeier B E E *et al* 1998 *J. Vac. Sci. Technol.* A **16** 2047
[4] Lee H C 2018 *Appl. Phys. Rev.* **5** 011108
[5] Godyak V 2013 *J. Phys. D: Appl. Phys.* **46** 283001
[6] Huang S *et al* 2018 *J. Vac. Sci. Technol.* A **36** 021305
[7] Kim J H *et al* 2003 *Appl. Phys. Lett.* **83** 4725
[8] You K H *et al* 2013 *Thin Solid Films* **547** 250
[9] Kim J H *et al* 2011 *Metrologia* **48** 306
[10] Lieberman M A and Lichtenberg A J 2005 *Principles of Plasma Discharges and Materials Processing* 2nd edn (Hoboken, NJ: Wiley)
[11] Tsendin L D 2010 *Phys. Usp.* **53** 133
[12] Godyak V A and Piejak R B 1993 *Appl. Phys. Lett.* **63** 3137
[13] Lee H C, Lee M H and Chung C W 2010 *Appl. Phys. Lett.* **96** 041503
[14] Lee H C and Chung C W 2013 *Phys. Plasmas* **20** 101607
[15] Lee H C and Chung C W 2015 *Phys. Plasmas* **22** 053505
[16] Lee H C *et al* 2013 *Phys. Plasmas* **20** 033504
[17] Szmytkowski C *et al* 2004 *Phys. Rev.* A **70** 032707
[18] Lisovskiy V *et al* 2014 *J. Phys. D: Appl. Phys.* **47** 115203
[19] Rescigno T N 1995 *Phys. Rev.* A **52** 329
[20] Dyatko N A and Napartovich A P 1999 *J. Phys. D: Appl. Phys.* **32** 3169
[21] Surendra M, Graves D B and Jellum G M 1990 *Phys. Rev.* A **41** 1112
[22] Song M Y *et al* 2017 *J. Phys. Chem. Ref. Data* **46** 043104
[23] Hamilton J R *et al* 2017 *Plasma Sources Sci. Technol.* **26** 065010
[24] Lee H C *et al* 2011 *Phys. Plasmas* **18** 023501
[25] Gangoli S P *et al* 2007 *J. Phys. D: Appl. Phys.* **40** 5140
[26] Shuo H *et al* 2017 *J. Vac. Sci. Technol.* A **35** 031302
[27] Barsukov Y *et al* 2017 *J. Vac. Sci. Technol.* A **35** 061310
[28] Mogab C J, Adams A C and Flamm D L 1978 *J. Appl. Phys.* **49** 3796
[29] Manos D M and Flamm D L 1989 *Plasma Etching: An Introduction* (London: Academic)